RSC Advances

PAPER

View Article Online
View Journal | View Issue

Cite this: *RSC Adv.*, 2017, **7**, 3870

Integration of Ag/AgCl and Au nanoparticles into isostructural porous coordination polymers of Ni(II), Co(II) and Mn(II): magnetic studies†

Rashmi A. Agarwal*[a] and Neeraj K. Gupta[b]

A systematic investigation of silver/silver chloride (Ag/AgCl) and gold (Au) nanoparticle (NP) formation within non-activated isostructural porous coordination polymers (PCPs) namely **Ni-PCP**, **Co-PCP** and **Mn-PCP** at room temperature is reported without the use of any reducing agent and deterioration of host frameworks. A supercharged environment due to the presence of free anions make these PCPs suitable templates for the growth of nanoparticles (NPs) in high yields. High resolution transmission electron microscopy (HRTEM) images provided insight into the size, shape and distribution of the NPs within the frameworks. Different shapes and sizes of the NPs are attributed to the differences in the levels of supramolecular interactions within these isostructural series and the ionic radii which is related to the charge density of metal nodes. From an electron paramagnetic resonance (EPR) study it is evidenced that synthesis of Au NPs in **Ni-PCP** is completely through redox reaction *via* strong charge transfer between coordinated metal and the metal precursor, and the others are *via* acid formation through anions present in the cavities of PCPs. Au NPs integrated frameworks display different soft ferromagnetic properties when placed in a magnetic field at room temperature.

Received 11th November 2016
Accepted 23rd December 2016

DOI: 10.1039/c6ra26642h

www.rsc.org/advances

Introduction

Porous coordination polymers (PCPs) or metal organic frameworks (MOFs) are crystalline materials which have permanent microporosity.[1–7] To achieve targeted properties in PCPs various types of multidentate organic ligands based on different geometries have been used with inorganic metal ions having a variety of coordination modes.[8] Large internal surface area, easy chemical modification of inner pore surface[9] and high thermal stability make these compounds excellent candidates for a variety of applications such as gas storage and separation,[10,11] heterogeneous catalysis[12] and proton conduction.[13] Recently there have been extensive studies to synthesize nanoparticles in PCPs due to their long range order of confined void space which act like reaction vessels. Free NPs tend to aggregate and fuse due to delocalization of free electrons[14] which increases their surface energies because of decreased thermodynamic stability. Due to aggregation their inherent properties disappear and storage is also affected from application point of view. That is why to nucleate NPs of uniform size and shape in homogeneous distribution pattern, encapsulation in microporous crystalline solids is an efficient way of preventing agglomeration.[15] Embedded NPs in the cavities of PCPs are very much of interest for applications in the field of heterogeneous catalysis,[16] gas storage,[17] chemical sensing,[18] electronics, biomedical assay (anticancer, antibacterial, antifungal and antimicrobial) and devices using quantum confinement effect.[19] Recently much attention has been paid to synthesis of plasmonic photocatalysts (Ag/AgCl) which are known to be an efficient and stable catalyst under irradiation of visible light in the field of environmental technology.[20] The fabrication of NPs in PCPs/MOFs can be achieved by a variety of methods including solution infiltration method where a solution of metal precursors in the form of inorganic salt are infiltrated into the pores of desolvated PCPs followed by reduction using reducing agents.[21,22] Another method involves chemical vapour deposition of volatile organometallic precursors into the inner surface of porous structure followed by thermal decomposition.[23] In a third process, double solvent approach where one solvent is hydrophilic (small amount) with metal precursor and the other is hydrophobic (large amount) with adsorbent are utilized with reduction at high temperature.[24] Other procedures involve solid grinding followed by hydrogenation[25] and photo catalytic reduction of metal precursors.[26]

Some of the above mentioned methods require high temperature while others require reducing agents. In particular redox active coordination polymers have attracted more attention since they react with metal precursors to produce oxidised frameworks and NPs at room temperature.[27] Their crystalline

[a]*Department of Chemistry, Indian Institute of Technology Kanpur, Uttar Pradesh 208016, India. E-mail: rashmi.a.agarwal@gmail.com*

[b]*Department of Mechanical Engineering, Indian Institute of Technology Kanpur, Uttar Pradesh 208016, India*

† Electronic supplementary information (ESI) available: EDS, EPR, TGA and HRTEM images. See DOI: 10.1039/c6ra26642h

nature is maintained even after the redox reaction. Recently Ag and Au NPs have been synthesized by reaction diffusion technique wherein anion alone or cooperatively with the framework reduce the metal precursors.[28] In this article we explore the nucleation and growth of NPs through acid formation *via* anion diffusion.

Herein we report the synthesis of Ag/AgCl and Au NPs from non-activated isostructural series of **Ni-PCP**, **Co-PCP** and **Mn-PCP** which are cationic frameworks wherein anions are free and fix their position *via* hydrogen bonding within the frameworks. During synthesis of Ag/AgCl NPs, NO_3^- anions of $AgNO_3$ are exchanged with free Cl^- anions in the frameworks followed by oxidation reaction by HCl formation and simultaneously metallic Ag is nucleated through reduction. HCl reacts instantaneously with Ag NPs to form AgCl NPs. While in case of Au NPs synthesis from $HAuCl_4$, Cl^- anions are exchanged with already present Cl^- anions to produce hydrochloric acid. This acid does not react with Au NPs.

Synthesis of Au NPs in **Ni-PCP** occurs through redox reaction between coordinated Ni(II) species of the framework and Au(III), as evidenced by EPR spectrum. In this case this PCP acts as a redox active framework. Differential ferromagnetic properties are shown by these Au NPs integrated frameworks at room temperature, which are influenced by size and distribution of the NPs.

Experimental

Materials

All chemicals and solvents used in the synthesis were of reagent grade and were used without further purification.

Physical measurements

Fourier transform infrared spectra (FTIR) were obtained (KBr disk, 400–4000 cm^{-1}) using a Perkin-Elmer model 1320 spectrometer. Solid-state diffuse reflectance spectra (DRS) were recorded using UV-vis-NIR spectrophotometer (Varian Model Cary 5000) at room temperature by using $BaSO_4$ as standard. EPR spectra were recorded on a Bruker EPR EMX spectrometer. Thermo-gravimetric analyses were recorded using a Mettler Toledo (heating rate of 10 °C min^{-1}) TGA instrument. Powder X-ray diffraction (PXRD) was performed using a Rigaku Rint 2000 X-ray diffractometer with CuKα radiation. X-ray photoelectron spectra were measured on a Sigma Probe. HRTEM images were obtained on a FEI Titan G2 60-300. The magnetic properties were analyzed on a LDJ9600 vibrating sample magnetometer.

Synthesis of isostructural PCPs

Ni-PCP $\{[Ni_2(DBIBA)_3]\cdot Cl\cdot 18H_2O\}_n$, $\{[Ni_2(DBIBA)_3]\cdot(ClO_4)\cdot 3H_2O\}_n$ **Co-PCP** $\{[Co_2(DBIBA)_3]\cdot Cl\cdot 9H_2O\}_n$ and **Mn-PCP** $\{[Mn_2(DBIBA)_3]\cdot Cl\cdot 3H_2O\}_n$ (DBIBA = 5-di(1*H*-benzo[*d*]imidazol-1-yl)-benzoate) were synthesized as previous reports.[10,11]

Synthesis of NPs@PCPs

All PCPs were used without activation or without guest removal, in powdered form (to increase their surface area). Solution infiltration methods were applied for NPs synthesis at room temperature.

Synthesis of Ag/AgCl@Ni-PCP

Ni-PCP $\{[Ni_2(DBIBA)_3]\cdot Cl\cdot 18H_2O\}_n$ (0.04 g, 0.026 mmol) was immersed in a methanol/water (3 mL, 2 : 1 v/v) solution of $AgNO_3$ (0.013 g, 0.078 mmol) at room temperature for 10 h under stirring. A brown coloured solid was filtered and washed several times with excess of methanol to remove any free $AgNO_3$. The solid material dried under vacuum. The obtained sample

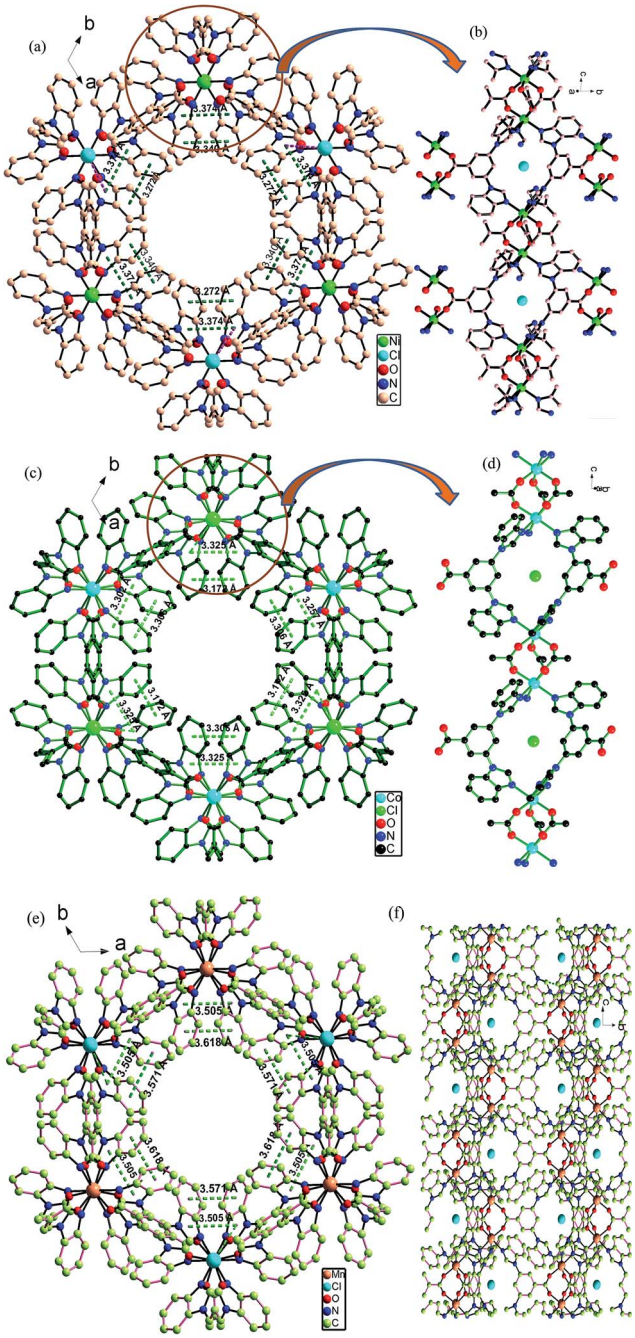

Fig. 1 Isostructural host PCPs with varying potential of electrostatic charges (a and b) **Ni-PCP**, (c and d) **Co-PCP** and (e and f) **Mn-PCP**.

has 32 wt% **Ag/AgCl@Ni-PCP** (the mass ratio of AgCl to **Ni-PCP** were 32%).

Synthesis of Ag/AgCl@Co-PCP

Co-PCP (0.04 g, 0.029 mmol) was immersed in a methanol/water (3 mL, 2 : 1 v/v) solution of $AgNO_3$ (0.015 g, 0.087 mmol) at room temperature for 10 h under stirring followed by same procedure. Here 33 wt% were acquired.

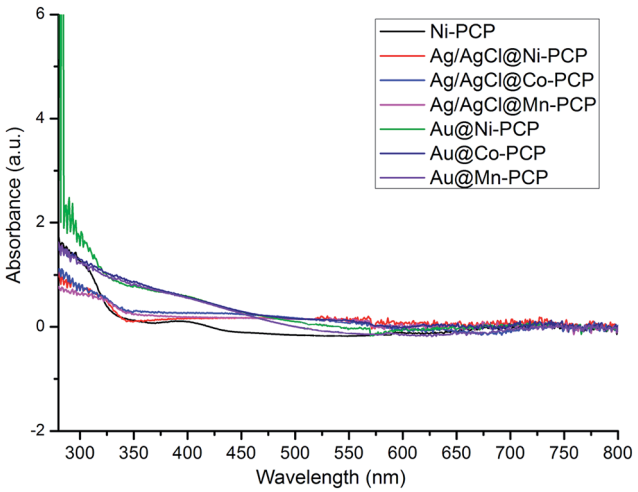

Fig. 2 UV-vis DRS spectra of **Ni-PCP**, **Ag/AgCl@Ni-PCP**, **Ag/AgCl@Co-PCP** and **Ag/AgCl@Mn-PCP**; and **Au@Ni-PCP**, **Au@Co-PCP** and **Au@Mn-PCP**.

Synthesis of Ag/AgCl@Mn-PCP

With similar method 25 wt% was prepared by using **Mn-PCP** (0.04 g, 0.031 mmol) and $AgNO_3$ (0.016 g, 0.093 mmol).

Synthesis of Au@Ni-PCP

In this case following $\{[Ni_2(DBIBA)_3]\cdot(ClO_4)\cdot 3H_2O\}_n$ was used as host framework with different anion. Same procedure was followed to synthesize 10 wt% **Au@Ni-PCP** with varying amount of **Ni-PCP** (0.04 g, 0.030 mmol) and $HAuCl_4$ (0.03 g, 0.09 mmol).

Synthesis of Au@Co-PCP

Here 6 wt% was obtained by utilizing **Co-PCP** (0.04 g, 0.029 mmol) and $HAuCl_4$ (0.029 g, 0.087 mmol).

Synthesis of Au@Mn-PCP

In this reaction **Mn-PCP** (0.04 g, 0.031 mmol) and $HAuCl_4$ (0.031 g, 0.093 mmol) were employed to obtain 21 wt% of **Au@Mn-PCP**.

Results and discussion

The isostructural series of PCPs comprising of Ni(II), Co(II) and Mn(II) nodes are thermally and structurally stable with permanent microporosity described through adsorption measurements. Slightly varying pore sizes and varying potential of different types of non-covalent interactions (π–π bonding between two benzene rings, hydrogen bonding by free anions, anion–π interactions and CH–π bonding) exist within their 1D

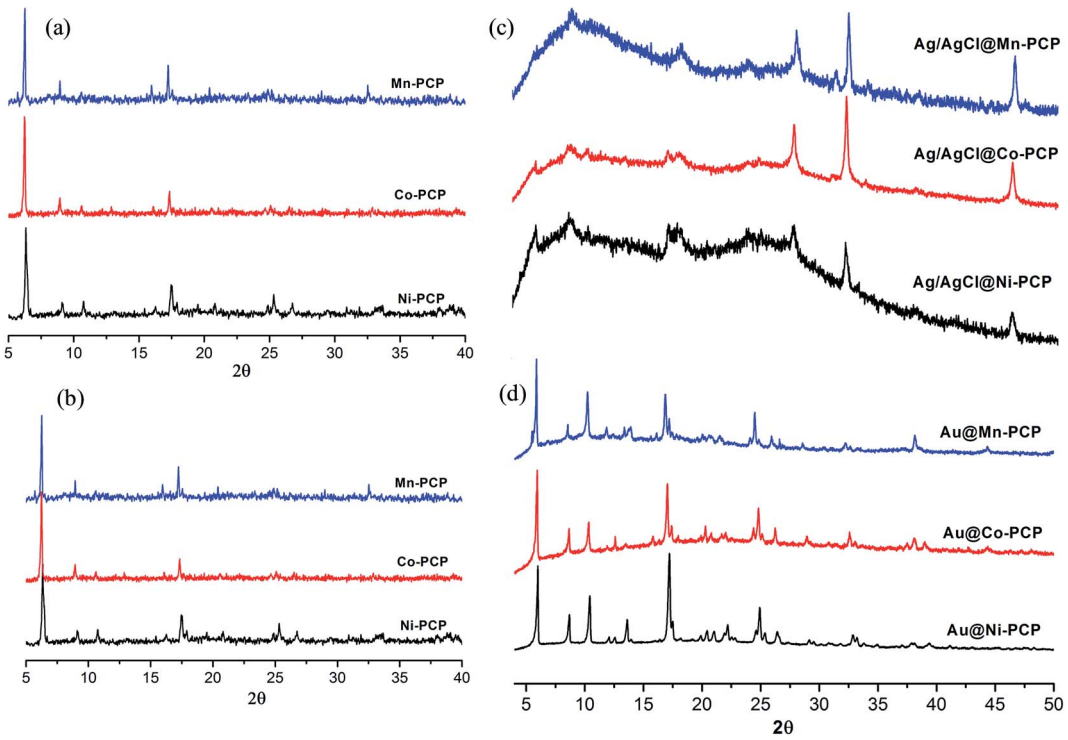

Fig. 3 PXRD patterns of (a) host PCPs, (b) PCPs after exposure to methanol/water solvent system for one day, (c) Ag/AgCl NPs integrated PCPs and (d) Au NPs integrated PCPs.

hexagonal cavities as previous reports.[10,11] These different types of supramolecular interactions with varying ranges are shown in Fig. 1a–f and Table S1.†

Their stable 3D structures and permanent microporosities with internally charged environment due to the presence of lattice anions (Cl^-) and varying potential of non-covalent interactions are suitable for nucleation, growth and storage of NPs. That is why these PCPs have been chosen for synthesis of NPs.

All three of the PCPs were immersed separately in methanol/water solvent system for 24 h to examine any structural changes. But PXRD patterns indicate (Fig. 3b) that there are no structural changes because these frameworks have been synthesized in ethanol/water solvent system. To fabricate Ag and Au NPs, these non-activated host PCPs were immersed, in suitable solutions of $AgNO_3$ and $HAuCl_4$ at room temperature for 10 h. Colour of the solutions were changed to brownish in case of Ag/AgCl loading indicating generation of surface plasma by Ag NPs whereas pale yellow colour appears in case of Au NPs integration. To check the deposition of NPs, characterizations have been done by diffuse reflectance spectroscopy (DRS), X-ray photoelectron (XPS) and Fourier transform infrared (FTIR) spectroscopy. High resolution transmission electron microscopy (HRTEM) and energy dispersive spectroscopy (EDEX) give information about morphology, size, distribution and coordination environment of NPs while structural changes of PCPs were analyzed through powder X-ray diffraction (PXRD) patterns after loading NPs.

From UV-visible diffuse reflectance spectra of **Ni-PCP** as well as synthesized **Ag/AgCl@Ni-PCP**, **Ag/AgCl@Co-PCP** and **Ag/AgCl@Mn-PCP** (Fig. 2), it is observed that broader and

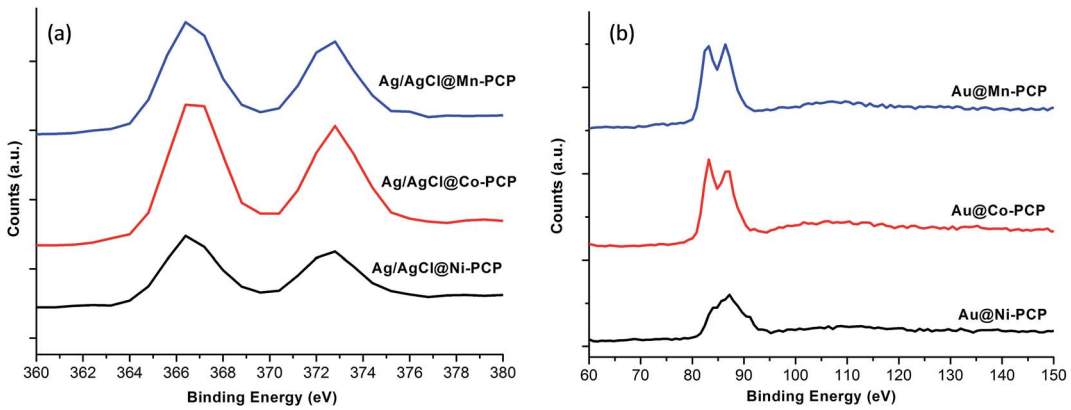

Fig. 4 XPS spectra of (a) Ag/AgCl fabricated PCPs and (b) Au NPs fabricated PCPs.

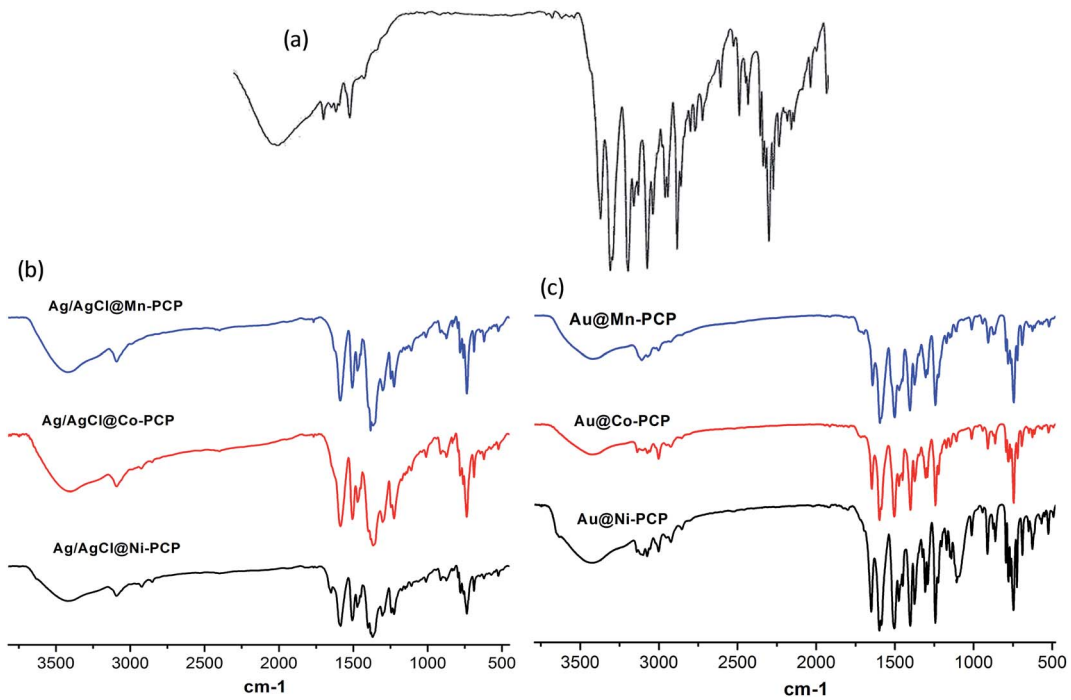

Fig. 5 FTIR spectra of (a) representative host PCP, (b) Ag/AgCl@PCPs and (c) Au@PCPs.

stronger absorptions in the visible-light region are due to the surface plasmon resonance of Ag NPs and unique heterojunction structures of Ag/AgCl NPs.[29]

To study the possible structural changes of PCPs before and after fabrication of NPs, PXRD patterns of **Ag/AgCl@Ni-PCP**, **Ag/AgCl@Co-PCP** and **Ag/AgCl@Mn-PCP** show that the host frameworks are stretched due to high loading of Ag/AgCl, yet maintaining their structural integrity (Fig. 3a and c). Prominent diffraction peaks at $2\theta = 27.8^\circ$, 32.3° and 46.3° are representative of face centered cubic structure of AgCl NPs.[30] A smaller peak at 38.1° corresponds to Ag NPs synthesis in [111] crystal plane. The low intensity of this peak infers that Ag NPs are of very small size. In comparison, the diffraction patterns of **Au@Ni-PCP**, **Au@Co-PCP** and **Au@Mn-PCP** (Fig. 3d) reveal that the host frameworks are not stretched to any appreciable degree and the 2θ peaks assigned to Au NPs indicate that the size is smaller than Ag/AgCl NPs.[31,32]

From XPS (Fig. 4) and EDS (ESI, Fig. S1†), it is evident that Ni–Ag, Ni–Au, Co–Ag, Co–Au, Mn–Ag and Mn–Au coexist within the frameworks forming nanocomposites. In XPS, $3d_{5/2}$ and $3d_{3/2}$ Ag(0) peaks are identified at 367.2 and 372.8 eV respectively, which are comparable to literature values.[33] These two peaks are further deconvoluted respectively in to two peaks at 366.4, 367.2 eV and 372, 372.8 eV. The peaks at 366.4 and 372 eV are ascribed to Ag^+ of AgCl NPs.[34] These results confirm the presence of both Ag/AgCl NPs in the frameworks. The peaks for Au(0), $4f_{7/2}$ and $4f_{5/2}$ exist at 83 and 86.5 eV comparable to literature values for all loaded PCPs.[35]

FTIR spectra (Fig. 5) of Ag/AgCl loaded PCPs show the presence of free NO_3^- at 1383 cm^{-1} which is due to acid formation

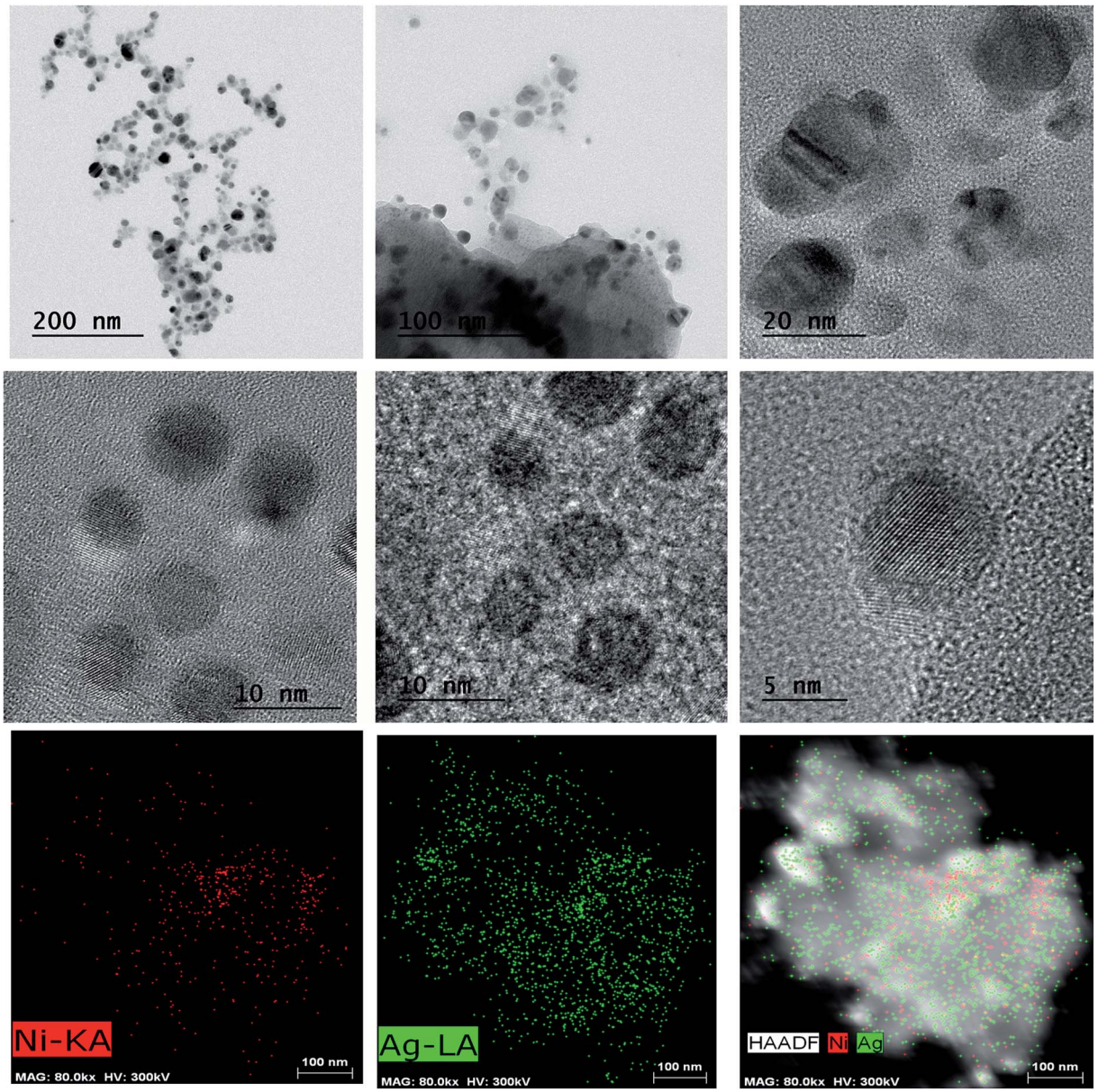

Fig. 6 HRTEM and HAADF-STEM images of **Ag/AgCl@Ni-PCP**.

(HCl) during anionic exchange. This evidences the synthesis of NPs within the frameworks. The spectral peaks of the host PCPs become broader and slightly shift toward lower wavenumbers inferring that Ag/AgCl NPs interact with the charged environment of the coordinated framework. The spectra of Au@PCPs indicate that there are no structural differences before and after Au NPs fabrication. Spectral peaks do not show any broadening nor any significant shifts. This shows that the NPs do not interact with the charged environment of the framework cavities. All the above spectra also support that the long range crystallinity of the frameworks are essentially intact.

EPR spectroscopy is sensitive to bulk properties of a sample. The strength of signals is indicative of NPs population throughout the bulk of the host frameworks. The spectra (ESI, Fig. S2 and S3†) for Ag/AgCl@PCPs shows g value in the range of 2.030–1.852 which indicates NPs of differing sizes. In comparison the spectra for Au@PCPs show a wider size distribution of Au NPs in the range $g = 2.042$–1.785. In the case of Ag/AgCl and Au@PCPs, except **Au@Ni-PCP**, the NPs are formed *via* acid formation during anion exchange between NO_3^- and Cl^- of $AgNO_3/HAuCl_4$ precursors and Cl^- of the frameworks. Redox activity of the framework in **Au@Ni-PCP** is evidenced by $g_{av} = 4.135$ for Ni(III) and ClO_4^- FTIR peak at 1090 cm^{-1}. In this redox active reaction Au(III) oxidises the coordinated Ni(II) to Ni(III) and get reduced to Au(0). This is due to strong charge transfer[36] between highly anisotropic Ni(II) and Au(III) because of higher ferromagnetic properties than **Co-PCP** and **Mn-PCP**.[11]

In **Au@Ni-PCP** this strong charge transfer mechanism can be potentially utilized for targeted drug delivery.

HRTEM images (Fig. 6 and 7, ESI, Fig. S4–S7†) taken at different magnifications show that the Ag/AgCl and AuNPs@PCPs essentially belong to class B wherein the NPs can

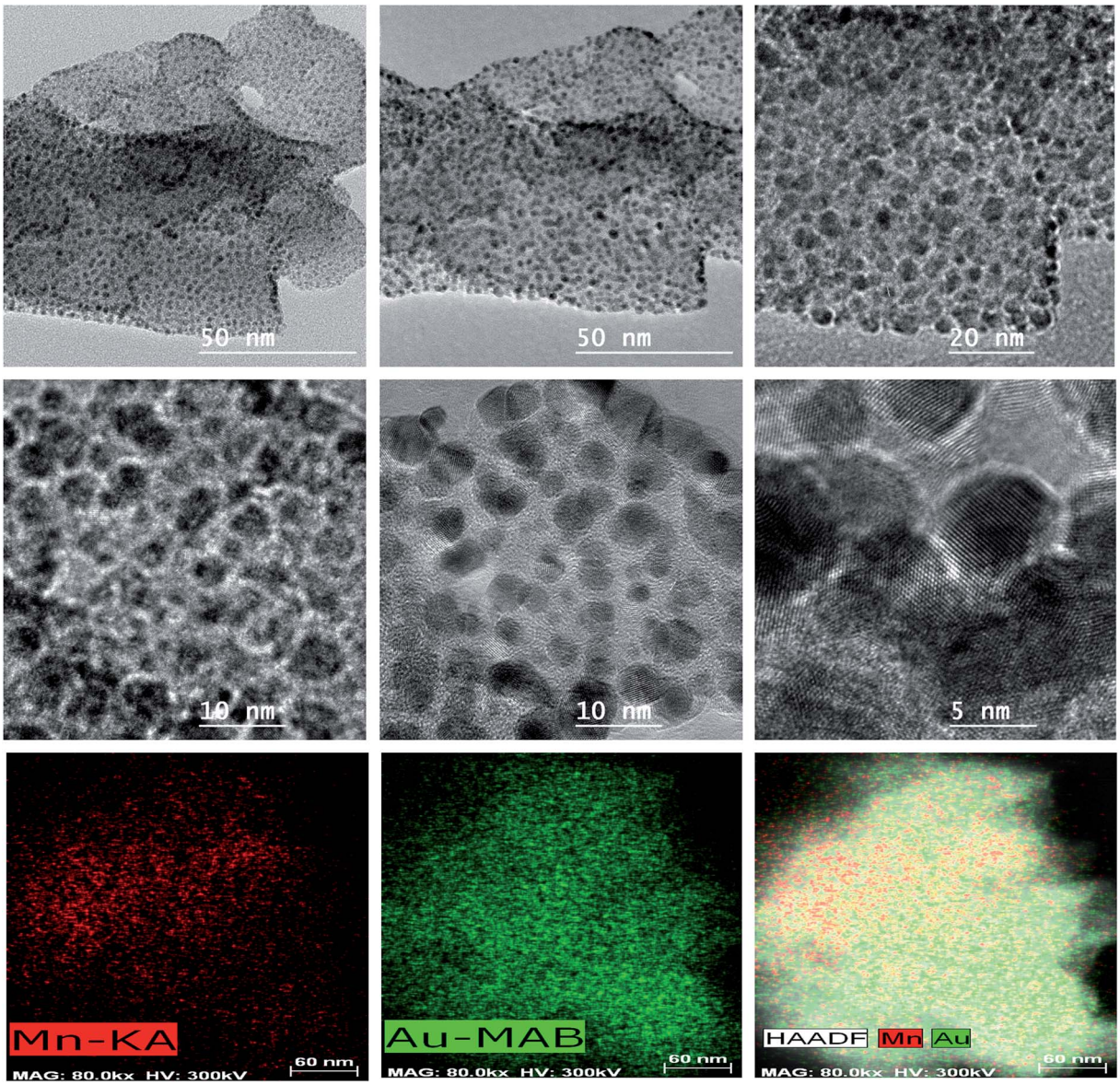

Fig. 7 HRTEM and HAADF-STEM images of **Au@Mn-PCP**.

be observed to be distributed homogeneously throughout the bulk of the crystalline frameworks with lattice fringes clearly visible. The shape of both type of NPs are essentially spheroids. The Ag/AgCl NPs in the isostructural frameworks are present in a broad size distribution with discrete particles 2–12 nm and nanoclusters 20–25 nm whereas in **Ag/AgCl@Mn-PCP** only discrete NPs exist. In the case of Au NPs, size range of discrete particles and nanoclusters are 1–6 nm and 8–20 nm respectively. However for **Au@Mn-PCP**, the NPs exist essentially as discrete particles in the range of 1–5 nm and no clusters. The size of fabricated NPs are much larger than the pore dimensions (0.65–0.71 nm) of the frameworks. Though the presence of NPs formed/deposited at the outer surface, which belong to class A is not ruled out, but is not the dominating phenomenon.[37] HAADF-STEM images provide chemical information proportional to atomic number of the metals present in the loaded frameworks. It is observed that besides the metal nodes, Ag/AgCl and Au nanoparticles/clusters are clearly visible with their distribution in the porous networks. Despite the difference between pore size and synthesized NPs, it is further evidenced that these NPs exist within the frameworks through the discussion of PXRD patterns wherein the frameworks are stressed by the larger than the pore size NPs.

Thermal and structural stabilities of Ag/AgCl and Au@PCPs were examined by thermo-gravimetry (ESI, Fig. S8†). For Ag/AgCl@PCPs there was almost constant weight loss upto ~95 °C which was attributed to removal of methanol which substitute water molecules (originally present in the PCPs) during NP synthesis. All these PCPs have significant thermal stability upto ~220 °C even though stabilities are decreased by ~150–180 °C in comparison to the host frameworks. This was ascribed to high stresses within the frameworks due to high wt% and catalytic activity of Ag NPs. For Au@PCPs, a constant weight loss upto ~80–90 °C was observed similar as for Ag/AgCl@PCPs. The Au@PCPs in comparison to Ag@PCPs show higher thermal stability even though they are lower by ~10–60 °C compared to their hosts.[38] It is inferred that these frameworks are less stressed as evidenced by PXRD. Despite the differences in thermal stabilities between the Ag/AgCl and Au@PCPs and host PCPs, the significant thermal stabilities of these systems show that the frameworks can be used as dry storage media for the NPs while preserving their inherent

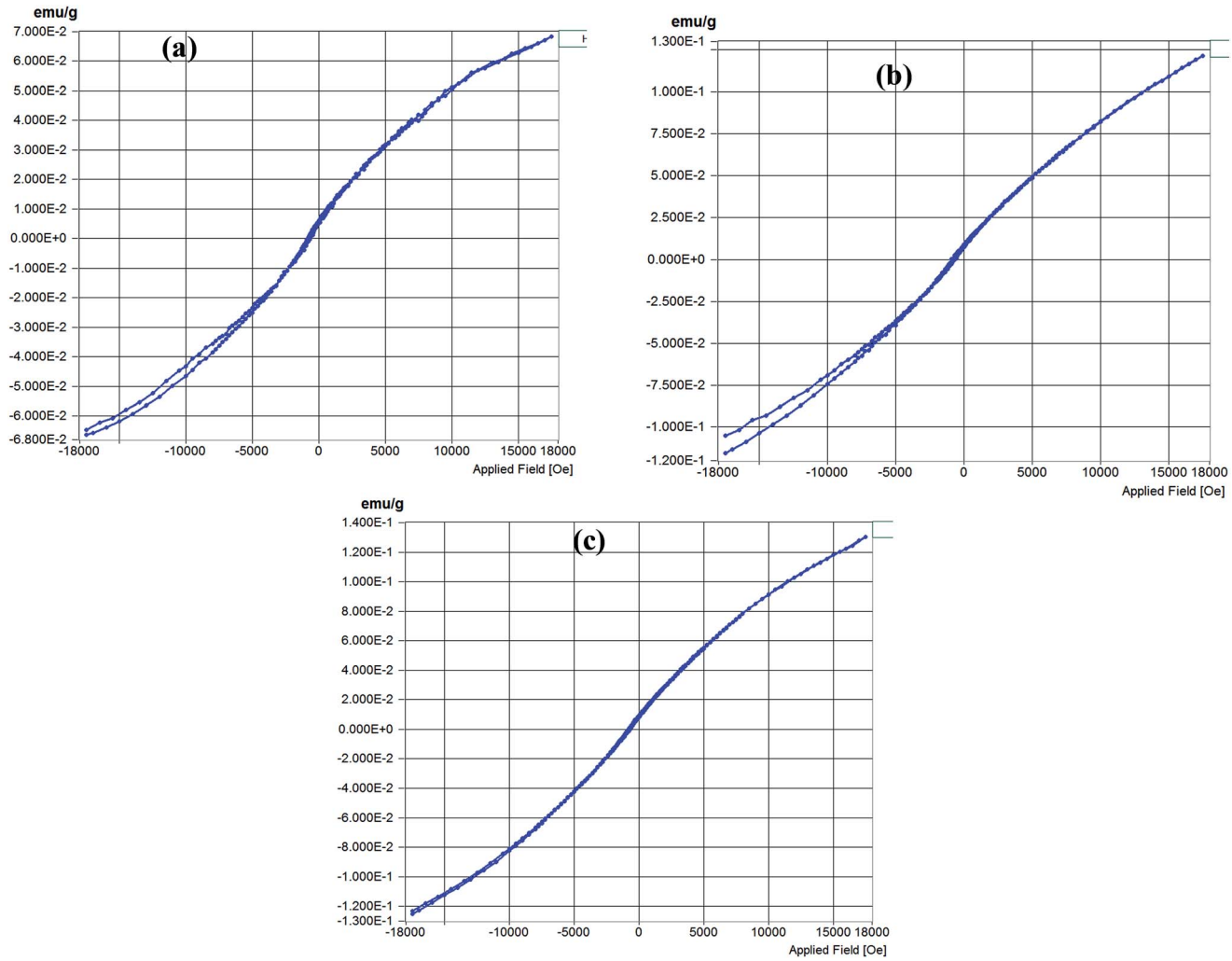

Fig. 8 Magnetic properties of Au NPs integrated frameworks (a) **Au@Ni-PCP**, (b) **Au@Co-PCP** and (c) **Au@Mn-PCP** at room temperature.

properties. Further the frameworks show potential for being used as templates for the re-fabrication of NPs for applications such as biomedical.

From the above discussions, it is clear that in case of **Ag/AgCl@Mn-PCP** and **Au@Mn-PCP** no nanoclusters are formed. The probable reasons for this are; (1) the higher torsion and dihedral angles N2Mn1O1C1 = 64.6(5), N1Mn1O1 = 65.07 for **Mn-PCP** compared to the other host PCPs (for **Ni-PCP**; N2Ni1O1C1 = −51.8(6), N1Ni1O1 = 58.22 and for **Co-PCP**; N2Co1O1C1 = 59.04, N1Co1O1 = 61.86) and (2) weaker electrostatic environment within the structure compared to the other two PCPs wherein the highly charged environment leads to agglomeration of NPs.

Magnetic measurements taken for **Au@Ni-PCP**, **Au@Co-PCP** and **Au@Mn-PCP** at room temperature up to 17 500 Oe are shown in Fig. 8. From the data it is seen that the coercive field (H_c) are 75.56, 105.28 and 61.90 Oe and remnant magnetization (M_r) 0.0002, 0.0007 and 0.0005 emu g^{-1} with saturation magnetization (M_s) values of 0.067, 0.12 and 0.13 emu g^{-1} respectively for the integrated frameworks. From the curves it is evident that these structures are soft ferromagnets or paramagnets. Further, **Au@Mn-PCP** and **Au@Co-PCP** show near comparable mass magnetization while **Au@Ni-PCP** shows the lowest value. The observed magnetism is attributed to both size and distribution patterns of the NPs within their respective frameworks. Since the above data has been generated on NPs integrated frameworks, we expect that the values would be higher with magnetic characteristics of hard ferromagnets if the NPs were free of their frameworks which act as non-magnetic barriers.

Conclusions

Conclusively we have demonstrated a very simple method of fabrication with different distribution patterns of Ag/AgCl and magnetic Au NPs in isostructural series of porous coordination polymers of Ni(II), Co(II) and Mn(II) in non-activated state. All NPs are synthesized due to hydrochloric acid formation through anion exchange between NO_3^- and Cl^- of $AgNO_3$/$HAuCl_4$ precursors and Cl^- of the frameworks. In **Au@Ni-PCP**, the framework shows redox activity due to strong charge transfer between coordinated Ni(II) and Au(III). Ag/AgCl and Au(0) fabricated PCPs are thermally stable. Integrated NPs show that their growth and distribution pattern depends on the charge density of the framework metal nodes and electrostatic gradients present. These isostructural PCPs show potential for the nucleation and growth of NPs from a variety of metal precursors. The Au NPs integrated frameworks display soft ferromagnetism at room temperature.

Conflict of interest

The authors declare no competing financial interest.

Acknowledgements

The authors would like to thank IIT Kanpur for extending facilities to undertake this study.

References

1 S. Kitagawa, R. Kitaura and S.-I. Noro, *Angew. Chem., Int. Ed.*, 2004, **43**, 2334–2375.
2 J. R. Long and O. M. Yaghi, *Chem. Soc. Rev.*, 2009, **38**, 1213–1214.
3 A. M. Spokoyny, D. Kim, A. Sumrein and C. A. Mirkin, *Chem. Soc. Rev.*, 2009, **38**, 1218–1227.
4 S. T. Meek, J. A. Greathouse and M. D. Allendorf, *Adv. Mater.*, 2011, **23**, 249–267.
5 J.-R. Li, J. Sculley and H.-C. Zhou, *Chem. Rev.*, 2011, **112**, 869–932.
6 H.-L. Jiang and Q. Xu, *Chem. Commun.*, 2011, **47**, 3351–3370.
7 Y. Sakata, S. Furukawa, M. Kondo, K. Hirai, N. Horike, Y. Takashima, H. Uehara, N. Louvain, M. Meilikhov, T. Tsuruoka, S. Isoda, W. Kosaka, O. Sakata and S. Kitagawa, *Science*, 2013, **339**, 193–196.
8 O. M. Yaghi, M. O'Keeffe, N. W. Ockwig, H. K. Chae, M. Eddaoudi and J. Kim, *Nature*, 2003, **423**, 705–714.
9 B. Moulton and M. J. Zaworotko, *Chem. Rev.*, 2001, **101**, 1629–1658.
10 R. A. Agarwal, A. Aijaz, M. Ahmad, E. C. Sañudo, Q. Xu and P. K. Bharadwaj, *Cryst. Growth Des.*, 2012, **12**, 2999–3005.
11 R. A. Agarwal, A. Aijaz, E. C. Sañudo, Q. Xu and P. K. Bharadwaj, *Cryst. Growth Des.*, 2013, **13**, 1238–1245.
12 S. Hasegawa, S. Horike, R. Matsuda, S. Furukawa, K. Mochizuki, Y. Kinoshita and S. Kitagawa, *J. Am. Chem. Soc.*, 2007, **129**, 2607–2614.
13 Y. Wang, Z. Tao, X. Yin, J. Shu, L. Chen, D. Sheng, Z. Chai, T. E. Albrecht-Schmitt and S. Wang, *Inorg. Chem.*, 2015, **54**, 10023–10029.
14 J.-T. Lue, *J. Phys. Chem. Solids*, 2001, **62**, 1599–1612.
15 R. J. White, R. Luque, V. L. Budarin, J. H. Clark and D. J. Macquarrie, *Chem. Soc. Rev.*, 2009, **38**, 481–494.
16 A. Corma, H. García and F. X. Llabrés i Xamena, *Chem. Rev.*, 2010, **110**, 4606–4655.
17 Y. E. Cheon and M. P. Suh, *Angew. Chem., Int. Ed.*, 2009, **48**, 2899–2903.
18 L. He, Y. Liu, J. Liu, Y. Xiong, J. Zheng, Y. Liu and Z. Tang, *Angew. Chem., Int. Ed.*, 2013, **52**, 3741–3745.
19 F. Cheng, J. W. Betts, S. M. Kelly, J. Schaller and T. Heinze, *Green Chem.*, 2013, **15**, 989–998.
20 H. Xu, H. M. Li, J. X. Xia, S. Yin, Z. J. Luo, L. Liu and L. Xu, *ACS Appl. Mater. Interfaces*, 2011, **3**, 22–29.
21 M. S. El-Shall, V. Abdelsayed, A. E. R. S. Khder, H. M. A. Hassan, H. M. El-Kaderi and T. E. Reich, *J. Mater. Chem.*, 2009, **19**, 7625–7631.
22 Y. K. Hwang, D.-Y. Hong, J.-S. Chang, S. H. Jhung, Y.-K. Seo, J. Kim, A. Vimont, M. Daturi, C. Serre and G. Férey, *Angew. Chem., Int. Ed.*, 2008, **47**, 4144–4148.
23 P. Serp, P. Kalck and R. Feurer, *Chem. Rev.*, 2002, **102**, 3085–3128.
24 A. Aijaz, A. Karkamkar, Y. J. Choi, N. Tsumori, E. Ronnebro, T. Autrey, H. Shioyama and Q. Xu, *J. Am. Chem. Soc.*, 2012, **134**, 13926–13929.
25 T. Ishida, M. Nagaoka, T. Akita and M. Haruta, *Chem.–Eur. J.*, 2008, **14**, 8456–8460.

26 R. Ameloot, M. B. J. Roeffaers, G. D. Cremer, F. Vermoortele, J. Hofkens, B. F. Sels and D. E. De Vos, *Adv. Mater.*, 2011, **23**, 1788–1791.
27 M. P. Suh, H. R. Moon, E. Y. Lee and S. Y. Jang, *J. Am. Chem. Soc.*, 2006, **128**, 4710–4718.
28 Y. Wei, S. Han, D. A. Walker, P. E. Fuller and B. A. Grzybowski, *Angew. Chem., Int. Ed.*, 2012, **51**, 7435–7439.
29 S.-T. Gao, W.-H. Liu, N.-Z. Shang, C. Feng, Q.-H. Wu, Z. Wang and C. Wang, *RSC Adv.*, 2014, **4**, 61736–61742.
30 L. Li and Y.-J. Zhu, *J. Colloid Interface Sci.*, 2006, **303**, 415–418.
31 Z. Ban, Y. A. Barnakov, F. Li, V. O. Golub and C. J. O'Connor, *J. Mater. Chem.*, 2005, **15**, 4660–4662.
32 H. R. Moon, J. H. Kim and M. P. Suh, *Angew. Chem.*, 2005, **117**, 1287–1291; *Angew. Chem., Int. Ed.*, 2005, **44**, 1261–1265.
33 P. Wang, B. Huang, Z. Lou, X. Zhang, X. Qin, Y. Dai, Z. Zheng and X. Wang, *Chem.–Eur. J.*, 2010, **16**, 538–544.
34 M. Zhu, P. Chen and M. Liu, *ACS Nano*, 2011, **5**(6), 4529–4536.
35 Z. R. Yue, W. Jiang, L. Wang, H. Toghiani, D. Gardner and C. U. Pittman, *Carbon*, 1999, **37**, 1607–1618.
36 W. S. Alencar, F. N. Crespilho, M. V. A. Martins, V. Zucolotto, O. N. Oliveira Jr and W. C. Silva, *Phys. Chem. Chem. Phys.*, 2009, **11**, 5086–5091.
37 M. Meilikhov, K. Yusenko, D. Esken, S. Turner, G. V. Tendeloo and R. A. Fischer, *Eur. J. Inorg. Chem.*, 2010, 3701–3714.
38 B. Gole, U. Sanyal, R. Banerjee and P. S. Mukherjee, *Inorg. Chem.*, 2016, **55**, 2345–2354.